Contrib. Astron. Obs. Skalnaté Pleso **39**, 85 – 100, (2009)

A probe to the Oort-cloud dynamics during an encounter of a dense condensation of giant molecular cloud

M. Jakubík and L. Neslušan

Astronomical Institute of the Slovak Academy of Sciences
059 60 Tatranská Lomnica, The Slovak Republic,
(E-mail: mjakubik@ta3.sk, ne@ta3.sk)

Received: June 3, 2009; Accepted: September 23, 2009

Abstract. The distant comet reservoir, Oort cloud, is perturbed by the Galactic tide, nearly passing stars, and giant interstellar molecular clouds. The perturbations by the latter are least frequent, but their amplitude is expected to be highest. In this work, we consider two models of a dense region of a giant molecular cloud and investigate its gravitational effect on the cometary Oort cloud, when the Solar System passes through. Since the comets in the Oort cloud prevailingly move in orbits with high galactic inclinations, we consider two geometries of the encounter differing in this aspect. Since the outer border of a relatively concentrated part of the real Oort cloud is estimated at ∼50 000 AU in terms of the semi-major axis, a, its passage through the central region of a giant molecular cloud does not, according to our simulations, significantly erode the Oort cloud. Although, it can change its structure for $a \gtrapprox 10^{4.4}$ AU. In our simulations, some changes depend on the model considered. For the Plummer model, the giant-molecular-cloud gravity caused an enlargement of the dispersion of galactic inclination and is selective to the specific values of the galactic argument of perihelion.

Key words: Oort cloud – giant molecular clouds – Plummer model

1. Introduction

It is well-known that the majority of comets are situated in the distant reservoir of these bodies, which is known as the Oort Cloud (OC). In the OC, comets are perturbed by several so-called outer perturbers. Besides the usual dominant perturbation by the Galactic tide, comet trajectories are influenced by the nearly passing alien stars and interstellar matter concentrated into the interstellar clouds.

Among the interstellar clouds, giant molecular clouds (GMCs) have been, especially, assumed to be the objects that could significantly perturb the OC comets. Bierman (1978) found that the outer part of OC can considerably be depleted due to the collisions with the interstellar clouds. Napier & Staniucha (1982) and Clube & Napier (1984) attempted to prove that the outer region of the OC, beyond ∼10 000 AU, was completely destroyed, so far, when the

Solar System (SS) encountered the GMCs or their substructures. At the same time, a new population of comets is captured from the GMCs (or, alternatively, the comets were drawn to the outer region from the inner comet cloud, below ∼10 000 AU). They estimated the number density of comets in the GMCs to be about 10^{-1} AU^{-3}. Other authors (e.g. Hut & Tremaine, 1985; Bailey, 1986), however, objected that Napier & Staniucha and Clube & Napier overestimated or underestimated some parameters of a typical encounter of the SS with a GMC and demonstrated that the effect of GMCs on the OC is not so extreme.

Recently, Mazeeva (2004) considered three examples of GMCs consisting of several (25 and 7) condensations as well as a GMC with a uniform density distribution and demonstrated a large influence of the GMCs on the OC-comet dynamics, especially in the case of structured, multi-condensation GMCs.

Despite the works mentioned above, the structure of the GMCs and their efficiency to perturb the OC-comet orbits remain uncertain. Mostly, this fact has caused that no GMC perturbations have been considered in the modelling of the OC formation, the most recent results including (Duncan et al., 1987; Dones et al., 2004; Brasser et al., 2006; 2007; 2008; Dybczyński et al., 2008; Leto et al., 2008; Kaib & Quinn, 2008).

In our work, we probe an impact of a GMC gravity on the structure of the OC. Specifically, we study the impact in the case, when the SS flies through a relatively dense region of a GMC, which is approximated by simplified models, in this paper. (We refer to this dense region as "condensation", hereinafter.) All combinations of two models of the GMC condensation and two geometries of the passage are considered.

2. About the observed structure of GMCs

Rosolowsky (2007) observed the GMCs in the nearby galaxy M31. In the table of GMC properties, presented in his paper, the deconvolved radii range from 19 to 92 pc and derived masses from 1.5×10^5 to 7.8×10^5 M$_\odot$.

The GMCs use to be identified and their internal structure uses to be studied from CO emission contours (e.g. Solomon et al., 1987). The GMCs are usually characterized by the total mass and effective radius. The latter is the radius of a hypothetical sphere containing all mass of the given GMC. In the given context, a spherical distribution of the GMC density, ρ, is assumed and described by relation

$$\rho(p) = \rho_1 \left(\frac{R_1}{p} \right)^{\alpha}, \tag{1}$$

where p is the cloud-centric distance, R_1 is the maximum radius of the GMC, and ρ_1 is the density at R_1. The standard value of power-index α is 1. This value is, however, not strict. Solomon et al. (1987) demonstrated that the density distribution law with $\alpha = 2$ also fits well an observed photometric behaviour. From the point of view of a dynamical study, the important feature of the density law (1), empirically derived from the CO-emission photometry, is a truncation of the cloud at $p = R_1$, i.e. $\rho = 0$ for $p > R_1$. This yields an artificial discontinuity in the distribution of the GMC matter, which is unacceptable in any dynamical study.

A requirement that the density must decrease abruptly to zero or, at least, faster than $\propto r^{-2}$ is necessary because of too large mass situated outside of the sphere with radius R_1. In a more detail, this mass would be infinite, if we considered the distribution law (1) with $\alpha \leq 2$ from the centre of the GMC to infinity. If we identified the border of the GMC with the distance, at which the density would decrease down to a common inter galactic density, $\sim 10^{-22}\,\mathrm{kg\,m^{-3}}$, then this "outer" mass would still exceed the mass inside radius R_1 by several orders of magnitude. For example, it would reach the value of $1.6 \times 10^9\,\mathrm{M_\odot}$ for the GMC with mass $5 \times 10^5\,\mathrm{M_\odot}$ being within $R_1 \approx 50\,\mathrm{pc}$. The density would decrease to the inter-galactic density at the distance of 734 pc. It is difficult to believe that such a matter, if actually existed, could evade detection.

When discussing the GMC structure, it is worth mentioning the theoretical deductions and a summary, at the same time, of some well-known properties of GMCs published by Williams et al. (2000). In the context of our work, they claimed, especially, that the structure of GMCs is fractal and, from the largest down to stellar-sized scale, the fractals are self-similar (except of the regions of an intensive star formation), i.e. the description of their structure can be approximated by the same matter-distribution law. The authors suggest that the density behaviour of the clumps inside the GMCs, if its shape is approximated by a sphere, can be described as proportional to $\propto r^{-2}$, i.e. $\alpha = 2$.

The observational facts mentioned above indicate that no suitable model of the GMC structure is known to provide an acceptable description of GMC's gravitational potential required in dynamical studies. The research of the dynamics of bodies in the GMC gravity must, thus, still rely on some simplified, theoretical models.

3. Categorization of encounters

A GMC is, typically, a complex of a number of various structures. These structures comprise large clouds of gas and dust, star-forming regions, hot dense cores, ridges, etc. Even if we knew a more precise and realistic description of a complex, the calculation of its gravitational potential would be consuming a computational-capacity and time beyond current technological capabilities. At present, it is impossible to compute the gravitational acceleration of every test particle (TP), in a model of the OC, in every orbit-integration time step for a whole period of several million years of the SS passage around or through the complex.

In the dynamical studies of the OC in a vicinity of a GMC, we are forced to approximate the effect of the GMC on the cometary nuclei. According to the increasing probability of occurrence of an encounter, it is appropriate to divide the encounter into three categories:

1. passages of the SS through a dense GMC condensation;
2. passages of the SS through an outer part of the complex;
3. distant passages of the SS around a GMC complex.

As mentioned in Sect. 1, we here deal with the first category.

4. The model of the Oort cloud

To characterize the magnitude of the perturbation by a GMC condensation (GMCC, hereinafter) better, we perform a few simulations, in which the OC comets are perturbed by GMCCs. The model of OC-comet orbits is created to be consistent with that obtained within the simulation of the OC formation, for 2 Gyr, performed by Dybczyński et al. (2008) and Leto et al. (2008). In the final stage, the distribution of eccentricity could be approximated, according to the output data obtained by Dybczyński et al. and Leto et al. (see http://www.astro.sk/∼mjakubik/AstroDyn/), as

$$N(e) = 29.4 \exp\left[-\frac{(e-0.945)^2}{2\times 0.0019}\right] + 4.8 \exp\left[-\frac{(e-0.945)^2}{2\times 0.1475}\right] \tag{2}$$

and that of galactic inclination as

$$N(i) = 37.5 \exp\left[-\frac{(i-84.8)^2}{2\times 15.6}\right] + 4.4 \exp\left[-\frac{(i-84.8)^2}{2\times 510}\right] \tag{3}$$

for the region of semi-major axis $a \geq 2000\,\mathrm{AU}$, where i is given in degrees.

To model specific orbits, we select 28 discrete values of eccentricity and 28 discrete values of inclination satisfying the distributions described by equations (2) and (3). In more detail, there are randomly generated 1, 1, 1, 2, 2, 4, and 17 discrete values of e in the intervals of $0.3-0.4$, $0.4-0.5$, $0.5-0.6$, $0.6-0.7$, $0.7-0.8$, $0.8-0.9$, and $0.9-1.0$, respectively. As well, there are randomly generated 1, 4, 20, 2, and 1 values of i in the intervals of 40^o-60^o, 60^o-80^o, 80^o-100^o, 100^o-120^o, and 120^o-140^o, respectively.

The galactic argument of perihelion, ω, and longitude of ascending node, Ω, of each modelled orbit are generated randomly in 12 equidistant sub-intervals of the entire interval spanning from 0^o to 360^o. Specifically, a discrete value of ω is randomly generated for 0^o-30^o interval, another value for 30^o-60^o interval, etc. The same generation procedure is performed to obtain 12 values of Ω. For a given value of the semi-major axis, the combination of all the above-described discrete values of e, i, ω, and Ω provides the modelled orbits of 112 896 TPs. The initial position of every test particle, representing a comet nucleus in the OC, is that in the aphelion of its modelled orbit.

Since we aim to study a possible disruption of the OC during the passage of the SS through a GMCC, we do not reduce the number of TPs at the outer border of the OC in accordance with the model by Dybczyński et al. and Leto et al., but we consider the same number of TPs for each considered discrete value of the TP-orbit semi-major axis. In the logarithmic scale, we choose 5 values of $\log_{10} a$ to map the influence of a GMC on the OC radial structure: $\log_{10} a = 4.1$, 4.4, 4.7, 5.0, and 5.3. Therefore, every simulation of the passage of SS through a given GMCC, described below, entails 564 480 TPs, in total. We do not suppose any significant influence of the GMCC on the deep interior of the OC, therefore the region with $\log_{10} a < 4.1$ is not considered.

With respect to the high abundance of high galactic inclinations, we consider two geometries (in the galactic coordinate system) of the penetration of the SS through the GMCC:

geometry I: cloud-centric z-coordinate of the Sun is *large* in comparison with its x- and y-coordinates at the minimum-proximity distance to the GMCC centre. The initial cloud-centric radius and velocity vectors of the Sun are chosen to be $\boldsymbol{p}_\odot = (8.39415476659495384 \times 10^7, 1.63165839848058000 \times 10^7, 1.50781884461960886 \times 10^7)$ AU and $\dot{\boldsymbol{p}}_\odot = (-1.32794083667699195 \times 10^{-2}, -2.34151798290726902 \times 10^{-3}, -2.37763967205307028 \times 10^{-3})$ AU day^{-1}.

geometry II: cloud-centric z-coordinate of the Sun is *small* in comparison with its x- and y-coordinates at the minimum-proximity distance to the GMCC centre. The initial cloud-centric radius vector of the Sun is identical to that in geometry I. The solar velocity vector is chosen, in this case, to be $\dot{\boldsymbol{p}}_\odot = (-1.31991223008173404 \times 10^{-2}, -2.54175032644409458 \times 10^{-3}, -2.60791855929692722 \times 10^{-3})$ AU day^{-1}.

With these initial geometries, the Sun passes the centre of the GMCC at minimum-proximity distance of 6.21 pc (1.28×10^6 AU). The simulation is started when the Sun is at the distance of 421 pc (8.68×10^7 AU) from the centre of the GMCC and finishes when the Sun, after passing the centre, again reaches this distance. The Sun moves along this trajectory during about 1.25×10^{10} days (34.2 million years).

We start and end the integration of solar motion in such the large GMCC-centric distance to avoid some artificial effects at a sudden emplacement of the Sun and OC into the GMCC gravitational potential. The action of the GMCC should start and "extinct" smoothly. Taking into account the structure of GMCC is important during a much shorter than the above-mentioned period. Namely, the gravity of structured GMCC is, practically, different from that of a point-like GMCC, when the SS is within the region of GMCC with a significantly high density gradient. In both considered GMCC models, such regions can be found within a distance of several parsecs from the GMCC centre (in the case of the Plummer model, see Sect. 5.3, this region is roughly within the Plummer radius being 8.42 pc (cf. this value with the solar-motion starting distance of 421 pc).

5. Modelling a GMC condensation

5.1. Purpose of the modelling

In this work, we perform a first step in our mapping of the GMCC perturbation on the OC considering two simplified models of the GMCC. The simplification assumes a smooth, single-law, density profile and the sphericity of the GMCC. One purpose of the simplification is a possibility to find some invariants of solar motion through the GMCC and, thus, to evaluate precisely the quality of the numerical integration at least for this massive body. Some more realistic models would likely provide qualitatively different results. Nevertheless, we believe that our present results achieved considering the simplified models are also beneficial.

The gravitational action of GMCC results in the accelerations of a given TP and the Sun. If we investigate the TP, which is gravitationally bound to the Sun and situated in the phase-space of the OC, it is suitable to use the heliocentric coordinate frame. If the orbit of the TP in this frame becomes hyperbolic, it is clear that the TP is no longer any member of the OC and SS.

The acceleration of the given TP, due to the GMCC, in the heliocentric coordinate frame, can be calculated as the difference in the accelerations of both the TP in the GMCC-centric coordinate frame and the Sun in the GMCC-centric frame. Hereinafter, we refer to this difference in TP and Sun accelerations as "acceleration difference" or "AcDf".

To calculate the accelerations of the Sun and TPs, we need to accept a model of GMCC to determine the gravitational potential, in which the Sun and TPs move.

5.2. Model 1: density proportional to $r^{-\alpha}$

As mentioned in Sect. 2, the density behaviour within a GMCC, approximated by a spheroid, was suggested to be described by equation (1), on the basis of radio observations. In a precise study of the OC dynamics, we need to start following the SS motion at a large distance from the GMCC, where the perturbation is negligible. In such a study, the truncation of GMCC at the distance R_1 represents a problem, because some artificial effects would be expected to occur, if we assumed the Sun and its OC to cross the density discontinuity. Of course, no such a discontinuity is expected at a real GMCC, but the density behaviour for distances larger than R_1 is difficult to determine even in a theoretical way.

To avoid the truncation problem and to estimate the perturbation of a dense GMCC on the OC, let us approximately assume that the sphere of influence of a given GMCC has a radius $p_1 < R_1$. Then, we can integrate the motion of the SS bodies completely within the sphere of radius R_1 and, thus, avoid the discontinuity problem.

When the usual value $\alpha = 1$ of the index appearing in (1) is considered, we can easily show that the GMCC causes a constant acceleration on a SS object in a condensation-centric distance $p < R_1$ and, therefore, zero AcDf. Inside the sphere of radius R_1, the GMCC of this kind has no influence on the OC dynamics in the SS-barycentre coordinate system.

Within the approximation of the GMCC-density behaviour by the equation (1), the consideration of the index $\alpha = 2$, which is also acceptable (Solomon et al. 1987), seems to be more realistic. In the following, we try to justify the value of $\alpha = 2$ in a theoretical way. Namely, we can demonstrate that the proportionality $\propto p^{-2}$ between the GMCC density and the cloud-centric distance must occur in an isothermal GMCC, if its matter is, at least approximately, in the thermodynamical equilibrium during an investigated period. Our derivation of the density behaviour in this case is following.

According to Whitworth and Summers (1985), the collapse or expansion of a spherically symmetric, isothermal sphere can be described by the equations

$$\frac{\partial M_p}{\partial p} - 4\pi p^2 \rho = 0, \tag{4}$$

$$\frac{\partial M_p}{\partial t} + 4\pi p^2 \rho u = 0, \tag{5}$$

$$\frac{\partial u}{\partial t} + u\frac{\partial u}{\partial p} + \frac{GM_p}{p^2} + \frac{1}{\rho}\frac{\partial \chi}{\partial p} = 0, \tag{6}$$

$$\chi = v_o^2 \rho, \tag{7}$$

where M_p is the mass within the sphere of radius p, t is time, u is the velocity of the outward radial flux, χ is the pressure, and v_o is the isothermal sound speed. The latter can be given as $v_o = \sqrt{kT/\mu}$, where k is the Boltzmann constant, T is the gas temperature, and μ is its molecular weight. For a typical abundances of the constituents of interstellar gas, $\mu = m_H/(0.72/2 + 0.25/4) \doteq 2.367 m_H$ (m_H is the mass of the hydrogen atom).

Following Shu (1977), Whitworth and Summers re-wrote these equations with the help of dimensionless variable ξ defined by

$$p = \xi v_o t \tag{8}$$

and dimensionless quantities[1]

$$M_p = \frac{w v_o^3 t}{G}, \tag{9}$$

[1]Whitworth and Summers (1985) labelled dimensionless variable by x and dimensionless quantities by w, y, and z. Since we need symbols x, y, and z for other purpose, we use ξ, η, and ζ.

$$u = \eta v_o, \tag{10}$$

$$\rho = \frac{\zeta}{4\pi G t^2}. \tag{11}$$

The new equations are

$$\frac{d\eta}{d\xi} = \frac{(\xi - \eta)^2 \zeta - 2(\xi - \eta)/\xi}{(\xi - \eta)^2 - 1}, \tag{12}$$

$$\frac{d\zeta}{d\xi} = \frac{(\xi - \eta)\zeta^2 - 2(\xi - \eta)^2 \zeta/\xi}{(\xi - \eta)^2 - 1}, \tag{13}$$

$$w = (\xi - \eta)\zeta\xi^2. \tag{14}$$

If we further adopt the simplification that the inward or outward flux of the matter in the part of the GMCC, where the OC is situated, is constant during the whole period of our investigation of the OC dynamics, we can write $u = const.$ and, thus, $\eta = const.$. Consequently, $d\eta/d\xi = 0$ and, from relation (12), one gets

$$\xi - \eta = \frac{2}{\zeta\xi}. \tag{15}$$

Supplying this result into equation (13), we obtain

$$\frac{d\zeta}{d\xi} = -\frac{2\zeta}{\xi}. \tag{16}$$

Integrating this equation, we can demonstrate that $\zeta \propto \xi^{-2}$ and hence $\rho \propto p^{-2}$. In other words, the latter implies $\alpha = 2$ in equation (1).

Now, let us deal with the calculation of the gravitational acceleration. In this calculation, we are interested in the mass M_p within the sphere of radius p. Supplying $\xi - \eta$ given by relation (15) into equation (14), we easily find $w = 2\xi$. The latter in a combination with relations (9) and (8) gives

$$M_p = \frac{2v_o^2}{G} p. \tag{17}$$

Using the Newton gravitational law, we can express the acceleration of the Sun as well as a comet (or TP) in the mass-centre (i.e. GMCC-centre, in fact) coordinate frame. For the solar-acceleration vector, we can write

$$\ddot{\boldsymbol{p}}_\odot = -\frac{2v_o^2}{p_\odot^2} \boldsymbol{p}_\odot, \tag{18}$$

where $\boldsymbol{p}_\odot = (p_{\odot x}, p_{\odot y}, p_{\odot z})$ and $p_\odot = |\boldsymbol{p}_\odot|$.

Integrating Eqs.(18), we can obtain the invariants of the solar motion

$$\dot{p}_{\odot x} p_{\odot y} - \dot{p}_{\odot y} p_{\odot x} = C_{z1}, \tag{19}$$

$$\dot{p}_{\odot y} p_{\odot z} - \dot{p}_{\odot z} p_{\odot y} = C_{x1}, \tag{20}$$

$$\dot{p}_{\odot z} p_{\odot x} - \dot{p}_{\odot x} p_{\odot z} = C_{y1}, \tag{21}$$

and

$$\dot{p}_{\odot x}^2 + \dot{p}_{\odot y}^2 + \dot{p}_{\odot z}^2 + 4 v_o^2 \ln p_\odot = h, \tag{22}$$

which can be used to check the accuracy of the numerical integration.

The equations of TP motion in the GMCC-centre frame are

$$\ddot{\boldsymbol{p}} = -\frac{G M_\odot}{r^3} \boldsymbol{r} - \frac{2 v_o^2}{p^2} \boldsymbol{p}, \tag{23}$$

where $\boldsymbol{p} = (p_x,\, p_y,\, p_z)$, $p = |\boldsymbol{p}|$, $\boldsymbol{r} = (x, y, z)$, and $r = |\boldsymbol{r}|$. The heliocentric radius-vector of the TP, $\boldsymbol{r}$, is related to its GMCC-centric radius-vector, $\boldsymbol{p}$, as

$$\boldsymbol{r} = \boldsymbol{p} - \boldsymbol{p}_\odot. \tag{24}$$

For TPs, we however primarily need the vector of AcDf, i.e. the TP's SS-barycentre coordinates. Subtracting the acceleration of the Sun from that of a given TP, the AcDf vector is

$$\ddot{\boldsymbol{r}} = -\frac{G M_\odot}{r^3} \boldsymbol{r} + 2 v_o^2 \left(\frac{\boldsymbol{p}_\odot}{p_\odot^2} - \frac{\boldsymbol{p}}{p^2} \right). \tag{25}$$

In the specific model considered in the numerical simulation, velocity v_o is gauged in the way that the GMCC mass within the radius of 5×10^5 AU is $2.5 \times 10^5\, \mathrm{M}_\odot$.

5.3. Model 2: Plummer model

Another probe is the study of the SS passage through a dense GMCC, when the Plummer model (Plummer, 1911) is used to describe its potential. The Plummer potential of a spherically symmetric gaseous condensation, at distance p from its centre, is given by (see also Binney and Tremaine, 1987; Kroupa et al., 2001; see also Brasser et al., 2006, for usage in the context of the comet cloud)

$$\Phi(p) = \frac{G M_T}{\sqrt{p^2 + c^2}}, \tag{26}$$

where M_T is its total mass and c is the so-called Plummer radius. It can be used to scale the rate of how steeply the density of the condensation rises toward its centre. The density behaviour is given as

$$\rho(p) = \frac{\rho_o}{\left(p^2 + c^2\right)^{5/2}}. \tag{27}$$

This implies that the mass within the sphere of radius p is

$$M_p = \int_0^p 4\pi p^2 \rho(p,c) dp = \frac{M_T p^3}{\left(p^2 + c^2\right)^{3/2}}. \tag{28}$$

The constant ρ_o is replaced by M_T realizing that

$$M_T = \int_0^\infty 4\pi p^2 \rho(p,c) dp = \frac{4\pi}{3}\rho_o c^3. \tag{29}$$

The equations of solar motion in the cloud-centric coordinate system are

$$\ddot{\boldsymbol{p}}_\odot = -GM_T \frac{\boldsymbol{p}_\odot}{\left(p_\odot^2 + c^2\right)^{3/2}}. \tag{30}$$

One can easily find four respective invariants of the solar motion:

$$C_z = \dot{p}_{\odot x} p_{\odot y} - \dot{p}_{\odot y} p_{\odot x}, \tag{31}$$

$$C_z = \dot{p}_{\odot y} p_{\odot z} - \dot{p}_{\odot z} p_{\odot y}, \tag{32}$$

$$C_z = \dot{p}_{\odot z} p_{\odot x} - \dot{p}_{\odot x} p_{\odot z}, \tag{33}$$

$$h_\odot = \frac{1}{2}\left(\dot{p}_{\odot x}^2 + \dot{p}_{\odot y}^2 + \dot{p}_{\odot z}^2\right) - \frac{GM_T}{\sqrt{p_\odot^2 + c^2}}, \tag{34}$$

which can be used to estimate the precision of the numerical integration of solar motion through the GMCC.

The heliocentric acceleration vector of the TP (i.e. TP's AcDf) can be written as

$$\ddot{\boldsymbol{r}} = -\frac{GM_\odot \boldsymbol{r}}{r^3} - GM_T \left[\frac{\boldsymbol{p}_\odot + \boldsymbol{r}}{\left(p_\odot^2 + 2\boldsymbol{p}_\odot \boldsymbol{r} + r^2 + c^2\right)^{3/2}} - \frac{\boldsymbol{p}_\odot}{\left(p_\odot^2 + c^2\right)^{3/2}}\right]. \tag{35}$$

We note that the transformation between the radius vectors of the TP in cloud-centric and heliocentric coordinate frames, $\boldsymbol{p}$ and $\boldsymbol{r}$, is given by relation (24).

In the specific model of the condensation introduced in this section, we consider the total mass of the GMCC to be $2.5\times10^5\,\mathrm{M}_\odot$ (the same as in Model 1) and the density in the centre equal to $\rho_c = 100\,\mathrm{M}_\odot\,\mathrm{pc}^{-3}$ ($6.77\times10^{-18}\,\mathrm{kg\,m}^{-3}$). This implies that the Plummer radius equals $c = [3M_T/(4\pi\rho_c)]^{1/3} = 8.42\,\mathrm{pc}$.

6. The results and their comparison

To estimate the amplitude of the perturbation of a GMCC on the OC and to map the change of the OC structure, we perform the integration of motion of all considered TPs (Sect. 4) for both chosen models of the GMCC (Sect. 5)

Table 1. The amounts (in percent) of the TPs with the given value of initial semi-major axis, a, which remained bound to the SS after their passages around the GMCC having the structure described by Model 1 or Model 2. Two geometries of the passages, in the case of each model, are considered.

	Model 1		Model 2	
$\log_{10} a$	geom. I	geom. II	geom. I	geom. II
4.1	100.0	100.0	100.0	100.0
4.4	100.0	100.0	100.0	100.0
4.7	100.0	100.0	100.0	100.0
5.0	100.0	100.0	95.4	96.2
5.3	0.0	0.0	0.5	0.0

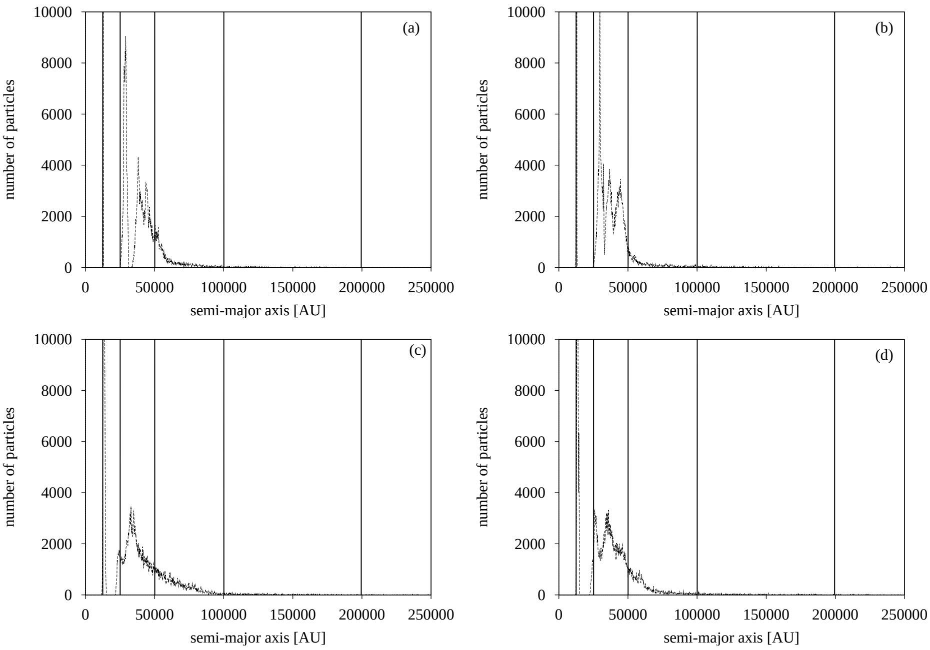

Figure 1. The distributions of the semi-major axes of the OC-comet orbits before and after the deep passage of the OC through the GMCC described by Models 1 (plots a and b) and 2 (c and d) for the geometries I (plots a and c) and II (b and d). The vertical solid lines indicate the initial values of a, before the passage. The dashed curves in the plots are the distributions after the passage.

and both chosen geometries (Sect. 4) of the passage. That is, we perform the simultaneous numerical integration of the equations of solar motion (18) and equations of TP motion (23) in the case of Model 1 and simultaneous numerical integration of the equations of solar motion (30) and equations of TP motion (35) in the case of Model 2. Each integration, irrespective of the model and geometry, is performed for the time of 1.25×10^{10} days (34.2 million years).

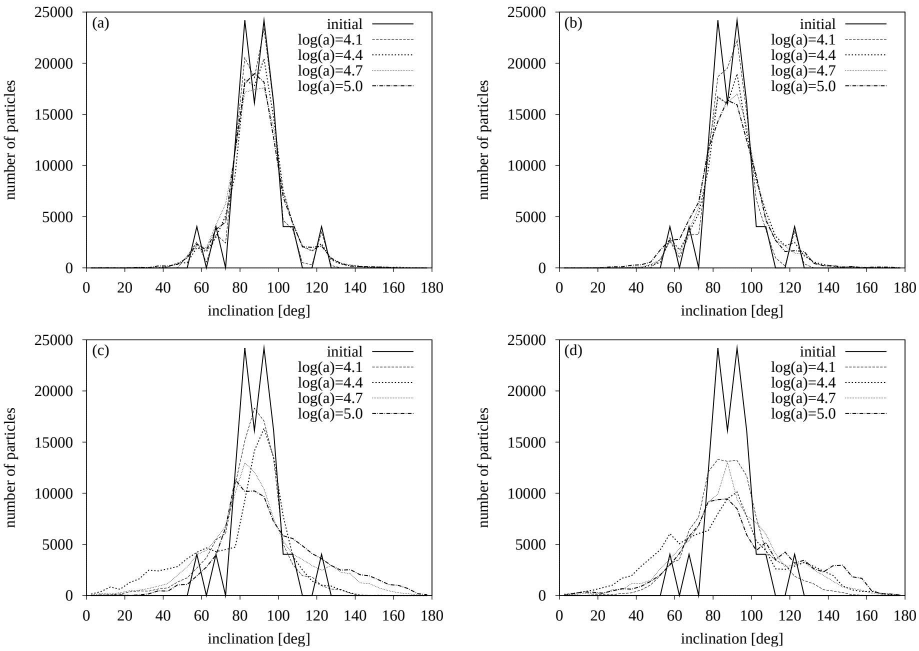

Figure 2. The distributions of the galactic inclination of the OC-comet orbits before (thick solid curve) and after (curves labelled in the plots) the deep passage of the OC through the GMCC described by Models 1 (plots a and b) and 2 (plots c and d) for the considered geometries I (plots a and c) and II (b and d).

The results of our simulations predict the following. The part of the OC comets in orbits with $a = 10^{5.3}$ AU, in this simulation, is completely stripped from the SS, regardless of the GMCC model or encounter geometry considered (Table 1). Almost all TPs in the orbits with $a = 10^{5.0}$ AU and shorter values of a survived the passage. Combining information in Table 1 and that in Fig. 1, we can conclude that the semi-major axes of all orbits having $a = 10^{5.0}$ AU are reduced. At least the outer-most surviving part of the OC shrinks due to the action of the GMCC. Thus, the OC contains only orbits with $a \lessapprox 90\,000$ AU after the passage. On the contrary, the OC-comet orbits seem to be untouched, if their semi-major axes are $a \lessapprox 10^4$ AU.

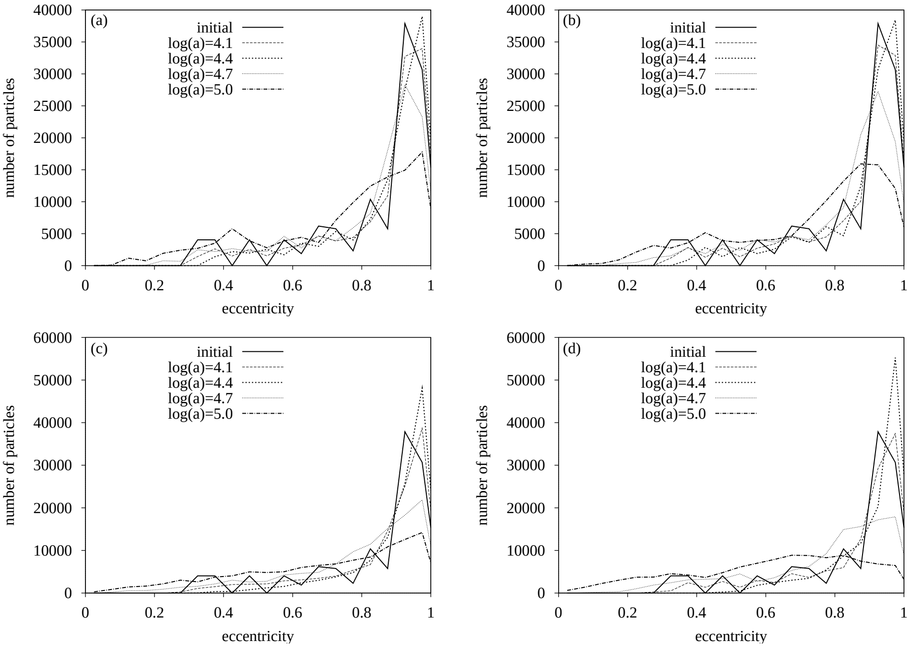

Figure 3. The distributions of the eccentricity of the OC-comet orbits before (thick solid curve) and after (curves labelled in the plots) the deep passage of the OC through the GMCC described by Models 1 (plots a and b) and 2 (plots c and d) for the geometries I (plots a and c) and II (plots b and d).

For Model 1, only a small part of the orbits having $a \sim 10^{4.4}$ AU is significantly perturbed by the GMCC in contrast to much larger changes in the case of Model 2. In Fig. 1a,b, we can further see that the outer border of the semi-major axis range is about ~60 000 AU for Model 1, both geometries, and ~70 000 AU for Model 2 and geometry II. A larger outer border of ~90 000 AU is found for Model 2 and geometry I.

It is well-known (e.g. Neslušan and Jakubík, 2005; Dybczyński et al., 2008) that a great majority of the OC orbits have a high galactic inclination. The peak of the i-distribution is centred at about 90^o. It is the effect of the action of Galactic tide. In Model 1, the encounter of the OC with a GMCC has almost no impact on this peaked structure (Fig. 2a,b). We can see a small change in the shape of the peak, but the dispersion of the inclination values is practically conserved. In Model 2 (Fig. 2c,d), the dispersion of the peak is enlarged for all considered values of initial semi-major axes.

The encounter causes a decrease of the orbital eccentricity for large values of semi-major axes ($\log_{10} a = 4.7$ and, especially, 5.0) for both considered models of GMCC (Fig. 3). For the lowest a ($\log_{10} a = 4.1$), the e-distribution is practically

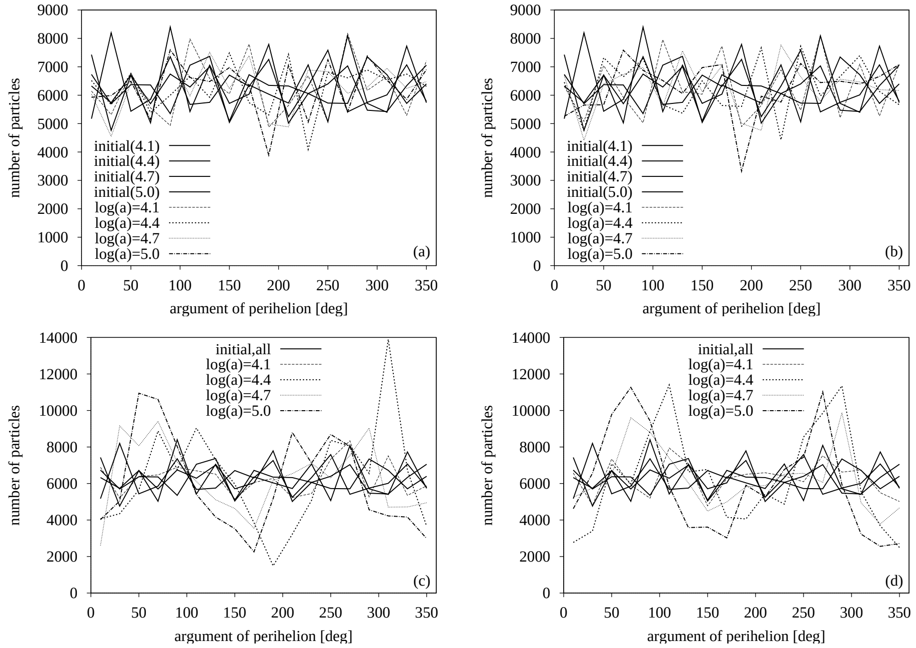

Figure 4. The distributions of the galactic argument of perihelion of the OC-comet orbits before (4 thick solid curves in each plot) and after (curves labelled in the plots) the deep passage of the OC through the GMCC described by Models 1 (plots a and b) and 2 (c and d) for geometries I (plots a and c) and II (b and d).

conserved for both models. As well, it is conserved for $\log_{10} a = 4.4$ and Model 1, both geometries. For Model 2, both geometries, and $\log_{10} a = 4.4$, the initial orbits become, statistically, more eccentric.

Finally, the action of the GMCC influences the distribution of the galactic argument of perihelion in the case of Model 2 (Fig. 4c,d): the relative abundance of orbits increases in intervals from $\sim 30^o$ to $\sim 90^o$ and from $\sim 240^o$ to $\sim 300^o$ and decreases from $\sim -70^o$ to $\sim +30^o$ and from $\sim 110^o$ to $\sim 240^o$. This change, however, does not concern the orbits with initial $\log_{10} a = 4.1$. For Model 1, no significant change in this distribution is found (Fig. 4a,b).

We note that the distribution of the galactic longitude of perihelion (not shown in any figure) is also slightly changed: the amplitude of its variation is detectably enlarged for the orbits with initial $\log_{10} a \geq 4.4$. An increase or decrease is not, however, related to any specific interval of the values of this element. The increase of the amplitude appears, here, regardless of the model or geometry considered.

7. Conclusions

Before summarizing the conclusions, it is necessary to note that we considered the simplified models of GMCCs, therefore the conclusions are rather indicative than definitive. Another future studies of this problem are still needed to clarify the role of the GMCs in the OC dynamics more. Based on our models and numerical integrations performed, the following can be stated.

Since the outer border of a relatively concentrated part of the real OC is estimated at ~50 000 AU in terms of the semi-major axis (only a small fraction of OC orbits has $a > 50\,000$ AU), the passage of the SS even through the central region of a GMCC does not, according to our simulations, significantly erode the OC, though it can change its structure for $a \gtrapprox 10^{4.4}$ AU. Regardless of the GMCC internal structure, the semi-major axes over this limit are reduced or enlarged. In our simulations, some changes depend on the model considered. For the Plummer model, the GMCC gravity causes an enlargement of the dispersion of galactic inclination and is selective to the specific values of the galactic argument of perihelion.

Acknowledgements. The authors thank the project "Enabling Grids for E-sciencE II" for the provided computational capacity. They also acknowledge the partial support of this work by VEGA − the Slovak Grant Agency for Science (grant No. 7047).

References

Bailey, M.E.: 1986, *Mon. Not. R. Astron. Soc.* **218**, 1
Biermann, L.: 1978, *Astron. Papers Dedicated to Bengt Strömgren, Symposium*, Copenhagen, 327
Binney, J., Tremaine, S.: 1987, *Galactic Dynamics*, Princeton Univ. Press, Princeton
Brasser, R., Duncan, M.J., Levison, H.F.: 2006, *Icarus* **184**, 59
Brasser, R., Duncan, M.J., Levison, H.F.: 2007, *Icarus* **191**, 413
Brasser, R., Duncan, M.J., Levison, H.F.: 2008, *Icarus* **196**, 274
Clube, S.V.M., Napier, W.M.: 1984, *Mon. Not. R. Astron. Soc.* **208**, 575
Dones, L., Weissman, P.R., Levison, H.F., Duncan, M.J.: 2004, in *Comets II*, ed.: M. C. Festou, H. U. Keller, and H. A. Weaver, Univ. Arizona Press, Arizona, 153
Duncan, M., Quinn, T., Tremaine, S.: 1987, *Astron. J.* **94**, 1330
Dybczyński, P.A., Leto, G., Jakubík, M., Paulech, T., Neslušan, L.: 2008, *Astron. Astrophys.* **487**, 345
Hut, P., Tremaine, S.: 1985, *Astron. J.* **90**, 1548
Kaib, N.A., Quinn, T.: 2008, *Icarus* **197**, 221
Kroupa, P., Aarseth, S., Hurley, J.: 2001, *Mon. Not. R. Astron. Soc.* **321**, 699
Leto, G., Jakubík, M., Paulech, T., Neslušan, L., Dybczyński, P.A.: 2008, *Mon. Not. R. Astron. Soc.* **391**, 1350
Mazeeva, O.A.: 2004, *Solar System Res.* **38**, 325
Napier, W.M., Staniucha, M.: 1982, *Mon. Not. R. Astron. Soc.* **198**, 723
Neslušan, L., Jakubík, M.: 2005, *Astron. Astrophys.* **437**, 1093
Plummer, H.C.: 1911, *Mon. Not. R. Astron. Soc.* **71**, 460

Rosolowsky, E.: 2007, *Astrophys. J.* **654**, 240
Shu, F.H.: 1977, *Astrophys. J.* **214**, 488
Solomon, P.M., Rivolo, A.R., Barrett, J., Yahil, A.: 1987, *Astrophys. J.* **319**, 730
Whitworth, A., Summers, D.: 1985, *Mon. Not. R. Astron. Soc.* **214**, 1
Williams, J.P., Blitz, L., McKee, C.F.: 2000, in *Protostars and Planets IV*, eds.: V. Mannings, A.P. Boss and S.S. Russell, Univ. Arizona Press, Tucson, 97